Received April 27, 2021, accepted May 7, 2021, date of publication May 13, 2021, date of current version May 24, 2021.

Digital Object Identifier 10.1109/ACCESS.2021.3079965

Isolation Enhancement of a Metasurface-Based MIMO Antenna Using Slots and Shorting Pins

MD. ABU SUFIAN[1], (Graduate Student Member, IEEE), NIAMAT HUSSAIN[1], HUSSAIN ASKARI[1], SEONG GYOON PARK[2], KOOK SUN SHIN[3], AND NAM KIM[1]

[1]School of Information and Communication Engineering, Chungbuk National University, Cheongju 28644, South Korea
[2]Department of Information and Communication Engineering, Kongju National University, Gongju 314701, South Korea
[3]FITI Testing & Research Institute, Cheongju 28115, South Korea

Corresponding author: Nam Kim (namkim@chungbuk.ac.kr)

This work was supported in part by the Institute for Information and Communication Technology Promotion (IITP) (A study on public health and safety in a complex EMF environment) under Grant 2019-0-00102, and in part by the Radio Research Agency (RRA) (Development of rapid antenna measurement technique for antennas with new radio technology).

ABSTRACT In this paper, a metasurface-based multiple-input multiple-output (MIMO) antenna with high isolation between antenna elements is presented. The main patch radiator is sandwiched between a metasurface and a ground plane to achieve performance enhancement. The fabricated single element antenna has a compact size of $0.85\lambda_0 \times 0.85\lambda_0 \times 0.038\lambda_0$. The antenna exhibits a wideband operational bandwidth from 3.27 to 3.82 GHz for $|S_{11}| < -10$, which corresponds to a fractional bandwidth of 15.5%. Moreover, stable radiation patterns with a peak gain of 8.1 dBi are also achieved across the operating band. The proposed single element antenna is characterized for 2×2 MIMO system by translating each antenna element orthogonal to each other. A decoupling structure consisting of slots and metallic strip with shorting pins is used to improve the isolation between the MIMO elements. The shorting pins connect the metallic strips (located between MIMO elements) on the metasurface and ground plane. These slots on ground plane and shorting pins affect the electromagnetic field distribution and consequently reduce the mutual coupling. The fabricated MIMO antenna has a compact size of $1.75\lambda_0 \times 1.75\lambda_0 \times 0.038\lambda_0$. The proposed 4 port ($2 \times 2$) MIMO antenna provides 15.9% of 10 dB impedance bandwidth from 3.3 to 3.87 GHz with a peak gain of 8.72 dBi. Moreover, the proposed MIMO antenna offers excellent diversity performance, isolation between antenna elements is very high (>32dB), ECC is lower than 0.001, and diversity gain is 9.99 dB very close to the ideal value of 10dB. Owing to these features, the proposed MIMO antenna can be a good candidate for 5G Sub-6 GHz (n78 band) smart devices and sensors.

INDEX TERMS Isolation enhancement, decoupling structure, slots, shorting pins, MIMO antenna, n78 band, sub-6 GHz, fifth-generation (5G), metasurface-based antenna.

I. INTRODUCTION

Fifth-generation (5G) wireless technology aims to provide higher peak data rates of multi-Gbps, ultra-low latency, huge network capacity, higher availability, and a more unified user experience [1]. Since 5G is seamlessly connected through modern technologies such as smart homes, smart factories, virtual reality, telemedicine, and automobiles, it is expected to bring a revolution in our daily lives [2]. Federal Communications Commission (FCC) classifies 5G spectrum into 4 bands [3]. The frequency spectrum from 1 – 6 GHz, is the mid-band spectrum, which is the ideal choice for the 5G mid-band because it can carry a large amount of data while also being able to transmit a long distance. For sub-6 GHz 5G communications systems, 3.3 – 3.8 GHz (n78 band) is the most used frequency range all over the world as shown in Fig. 1 [4].

The MIMO (Multiple-Input Multiple-Output) antennas are considered as a better candidate for 5G applications. The use of MIMO antenna is an effective way to improve link reliability and increase the spectral efficiency of radio communication [5]. The MIMO techniques enable the transmission of data over multiple channels and thus increase the channel capacity without additional power requirements [6]. MIMO antennas can be used for achieving diversity performance and mitigating the effects of multipath fading [7].

The associate editor coordinating the review of this manuscript and approving it for publication was Tutku Karacolak.

Countries	1 – 3 GHz Band	3 – 4 GHz Band	4 – 5 GHz Band
Korea	2.3 – 2.39 GHz	3.4 – 3.7 GHz, 3.7 – 4.0 GHz	
Japan		3.6 – 4.1 GHz	4.5 – 4.9 GHz
China	2.50/2.6 GHz (B41/n41)	3.3 – 3.6 GHz	4.5 – 5 GHz
EU		3.4 – 3.8 GHz	
UK		3.4 – 3.8 GHz	
Germany		3.4 – 3.8 GHz	
France		3.46 – 3.8 GHz	
Italy		3.6 – 3.8 GHz	
USA	2.50/2.6 GHz	3.45 – 3.7 GHz, 3.7 – 3.98 GHz	4.49 – 4.99 GHz
Canada		3.475 – 3.65 GHz, 3.65 – 4.0 GHz	
Australia		3.4 – 3.7 GHz	
India		3.3 – 3.6 GHz	

FIGURE 1. The global 5G sub-6 GHz mid-band spectrum [4].

One of the main challenges in MIMO antenna design is the isolation enhancement. Various types of isolation enhancement techniques have been reported [8]–[19]. By adopting different decoupling elements, the mutual coupling between antenna elements can be reduced [8]–[10], such as parasitic monopole [8], floating parasitic [9], and tree-like structure on the ground plane [10]. However, the antenna configurations in [9] and [10] are more complex and occupy much space. The T-shaped metallic strip between two antennas and rhombic slot structure in the ground plane is used to improve isolation [11]. The mutual coupling between patch radiators can also be reduced by using a polarization conversion isolator [12]. Whereas, polarization conversion isolator is placed between patch radiators which effectively reduces the influence of mutual coupling on the direction of the main beam. In [13], a pair of open-ended circular parasitic structures with a square-ring slot radiator is embedded, in order to reduce the mutual coupling of the antenna elements. Another effective way to reduce mutual coupling between MIMO antenna elements is the electromagnetic bandgap (EBG) [14]–[16]. EBG structures placed between MIMO antenna elements, cancel the undesired resonance between antenna elements. Therefore, the mutual coupling between antenna elements is reduced and high isolation is achieved. The uni-conductor electromagnetic bandgap (UC-EBG) periodic cells are placed between antennas which act as barriers for surface waves to provide high isolation [14]. Also in [15], fractal shape EBG structure has been considered to reduce the mutual coupling for the array antenna design. While a multi-layered electromagnetic bandgap (EBG) structure is incorporated into a MIMO antenna to reduce unexpected mutual coupling between antenna elements [16]. In addition, other isolation enhancement techniques are mentioned in the literature [17]–[19]. The metamaterial superstrate structure and mutual decoupling structure are used to reduce the mutual coupling [17]. A two-layered 3-D metamaterial structure connected by shorting pins has been proposed and it has been integrated into a MIMO antenna to reduce the mutual coupling between two rectangle patch antennas [18]. While, near-field resonators (NFR) are used to enhance the isolation between closely packed patch antennas in [19].

Recently, metasurface (MTS) has been intensively studied and utilized to improve the performance of microstrip patch antennas, especially bandwidth and gain [20]–[24]. The antenna in [20], is designed for 5G mm-wave applications, and to achieve the performance enhancements both the patch radiator and the periodic metallic plate metasurface are printed on the same dielectric layer. In [22]–[24], double-layered metasurface-based antennas for performance improvements especially in terms of gain and bandwidth are presented. This work is based on our previous work [22], where the concept of patch antenna sandwiched between a metasurface and a finite ground plane for 3.5 GHz application was presented.

In this article, a metasurface-based multiple-input multiple-output antenna is presented for 5G sub-6 GHz (n78 band) applications. The distinguishing feature of this design is high isolation between MIMO antenna elements while maintaining high gain and wideband characteristics. In this work, a decoupling structure consisting of slots and metallic strips with shorting pins is proposed to improve the isolation between the MIMO elements. By properly designing the configuration of the slots and shorting pins, high gain and high isolation between antenna elements are achieved. CST Microwave Studio is used as a tool for doing all the antenna simulations. The rest of the paper organization is as follows. In section 2, the antenna geometry of the proposed single element antenna, its design procedure, performance enhancement techniques, simulated and measured results are presented. While the design of the proposed MIMO antenna configuration, isolation enhancement, and its diversity parameters along with its performance comparison with other works is discussed in section 3 and section 4. Finally, the proposed work is concluded in section 5.

II. DESIGN AND CHARACTERIZATION OF THE SINGLE ELEMENT ANTENNA

The antenna geometry and design procedure of the single element antenna are explained in this section. Furthermore, the simulated and measured results including $|S_{11}|$, radiation efficiency, gain, and radiation patterns are studied in detail.

A. ANTENNA GEOMETRY

The geometry and configuration of the proposed single element antenna are shown in Fig. 2. The antenna consists of a radiating patch fed by a microstrip line, a ground plane, a metasurface, and two identical Rogers RO4003C substrates ($\varepsilon_r = 3.55$ and $tan\delta = 0.0027$) with the thickness of $h_1 = h_2 = 1.524$ mm. The microstrip line is fed by a 50-Ω coaxial cable. The radiating patch is a rectangular patch with the dimension of $W \times L$, whose lower ends are truncated with a semi-circle. The microstrip feed line has the width and length of W_f and L_f, respectively. The proposed metasurface is a uniform array of 4×4 metallic square cells. Each cell has a width of m and the gap between the nearest cells is g. The metasurface is printed on the top of the upper substrate, while the radiating patch is printed on the upper side of the lower substrate, and on the other side, the ground is printed. The patch is fed by the SMA connector by connecting the inner pin of the connector to the microstrip feed line that

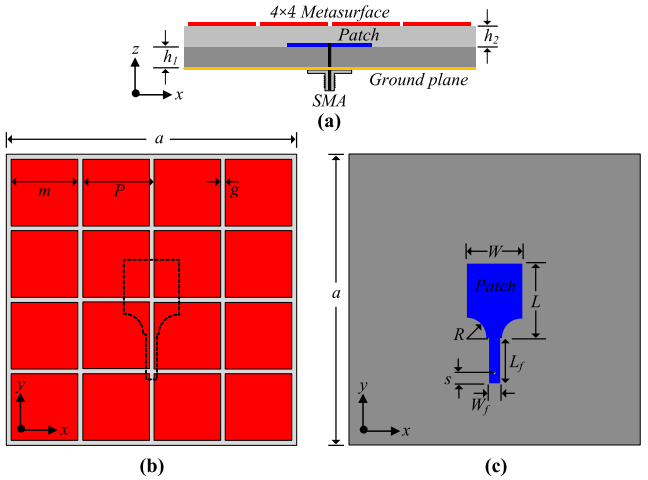

FIGURE 2. Geometry and configuration of the proposed single element antenna: (a) side view (b) top view of metasurface, and (c) top view of the patch.

passes through the lower substrate, while the outer part of the connector is soldered with the ground. The antenna has an overall size of 71.6 mm × 71.6 mm × 3.118 mm which corresponds to $0.85\lambda_0 \times 0.85\lambda_0 \times 0.038\lambda_0$, where λ_0 is the center operating frequency. The optimized parameters for the antenna are as: $a = 71.6$ mm, $L = 19$ mm, $W = 14.5$ mm, $h_1 = h_2 = 1.524$ mm, $R = 5$ mm, $L_f = 11.6$ mm, $W_f = 3$ mm, $s = 2$ mm, $m = 16.4$ mm, $P = 17.6$ mm, $g = 1.2$ mm.

B. DESIGN PROCEDURE AND PERFORMANCE ENHANCEMENT

The proposed double-layer sub-6 GHz 5G antenna based on metasurface is evolved from a microstrip-line fed rectangular patch antenna chosen to operate at the desired frequency of $f_r \approx 3.5$ GHz. The antenna is fed from the bottom side through a coaxial feed. Without metasurface dimension (W and L) of the initial patch may be predicted as [25]:

$$W = \frac{c}{2f_r}\sqrt{\frac{2}{\gamma_r + 1}} \tag{1}$$

$$L = \frac{c}{2f_r\sqrt{\gamma}_{reff}} - 2\Delta L \tag{2}$$

where c is the light velocity in free space, γ_r is the dielectric constant of the substrate, γ_{reff} is the effective dielectric constant of the patch and ΔL is the extended incremental length of the patch.

The optimized parameters for the antenna without metasurface are as: $a = 71.6$ mm, $L = 23$ mm, $W = 21$ mm, $h_1 = 1.524$ mm, $R = 5$ mm, $L_f = 13$ mm, $W_f = 0.4$ mm, $s = 2$mm. The metasurface layer printed on another substrate and placed on top of the radiating patch as in Fig. 2, in order to improve the antenna performance. The performance, especially operating bandwidth, and gain of the patch antenna are improved by utilizing periodic structure as MTS shown in Fig. 3. It is observed from the simulation result that

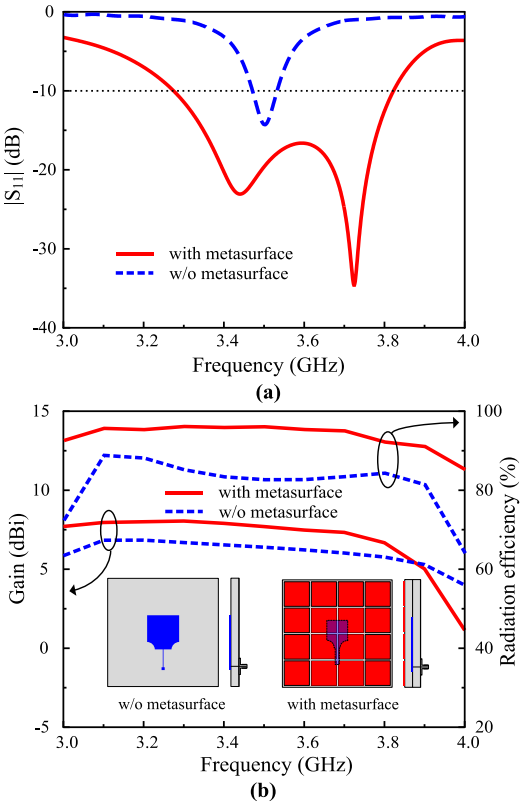

FIGURE 3. Simulated results of the proposed single element antenna with and without metasurface: (a) $|S_{11}|$, (b) gain and efficiency.

without metasurface structure, the antenna's impedance matching ($|S_{11}| < -10$dB) is from 3.45 to 3.53 GHz corresponds to a fractional bandwidth of 2.3% with respect to the center frequency. With metasurface structure, good impedance matching ($|S_{11}| < -10$dB) is obtained from 3.27 to 3.82 GHz corresponds to a fractional bandwidth of 15.5%. By using the metasurface structure, the bandwidth is increased by 13.2%. Without the metasurface structure, the peak gain in operating frequency is 6.3 dBi and radiation efficiency is less than 83%. While with metasurface structure, the peak gain in operating frequency is 8.1 dBi, and radiation efficiency is more than 92% (up to 96%).

The performance improvement of patch radiator using metasurface can be explained by surface wave propagation. The surface waves propagating on the metasurface generate additional resonances. These additional resonances are utilized effectively to increase bandwidth and gain, which have been thoroughly investigated in [20], [24], [26], [27].

C. RESULT AND DISCUSSION

A prototype of the proposed double-layer metasurface-based wideband antenna is fabricated and measured to verify the design concept. The photographs of its parts of assembly and the fabricated antenna, and the far-field measurement setup are shown in Fig. 4. With the help of an adhesive liquid, the MTS layer is directly stacked on the patch antenna. A 50-Ω 2.92mm K-connector is connected carefully with

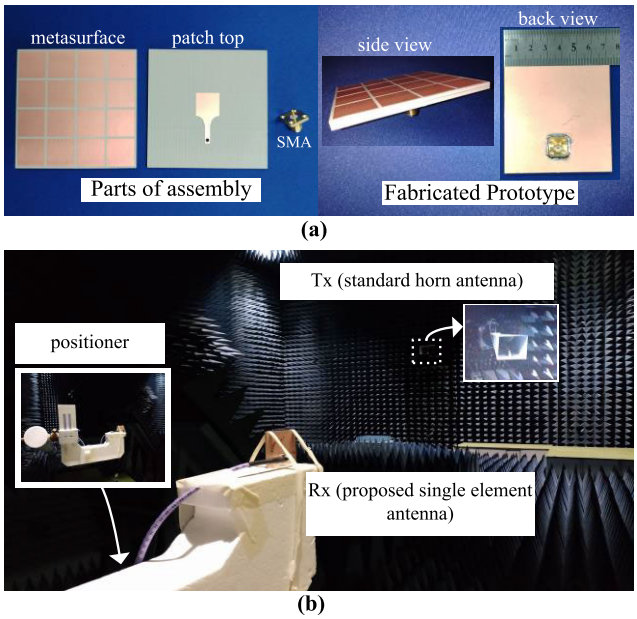

FIGURE 4. Photographs of the (a) fabricated single element antenna and its parts of the assembly, and (b) far-field measurements setup.

the feed line. PNA network analyzer (Agilent Technologies E8364B) was used to measure S-parameter in open-air condition and the far-field radiation performance is measured and characterized by a commercial company [28] in an anechoic chamber. A well calibrated standard gain horn antenna is used as a transmit (TX) antenna and the prototype is measured as a receiving (RX) antenna. Amplifiers are used to supply stable power reception. At the time of testing, the antenna is rotated to measure the radiation intensity at different orientations. In general, a good agreement between the simulated and measured results is observed.

1) REFLECTION COEFFICIENT ($|S_{11}|$)

The simulated and measured return loss ($|S_{11}|$) of the single element antenna with metasurface is shown in Fig. 5(a). Simulated and measured results show that the proposed single element antenna has a wide 10 dB impedance bandwidth of 15.5% (3.27 – 3.82 GHz). The wideband characteristics are obtained for the successful implementation of the metasurface.

2) RADIATION EFFICIENCY AND GAIN

Radiation efficiency and gain of the proposed single element antenna are shown in Fig. 5(b). The measured maximum value of the achieved gain is 8.1 dBi. Again the bandwidth and gain are increased due to the usage of MTS as a secondary radiator for useful extra resources. Due to connector/cable losses used during measurement, the measured gain and radiation efficiency are a little lower than the simulated values in the entire frequency range.

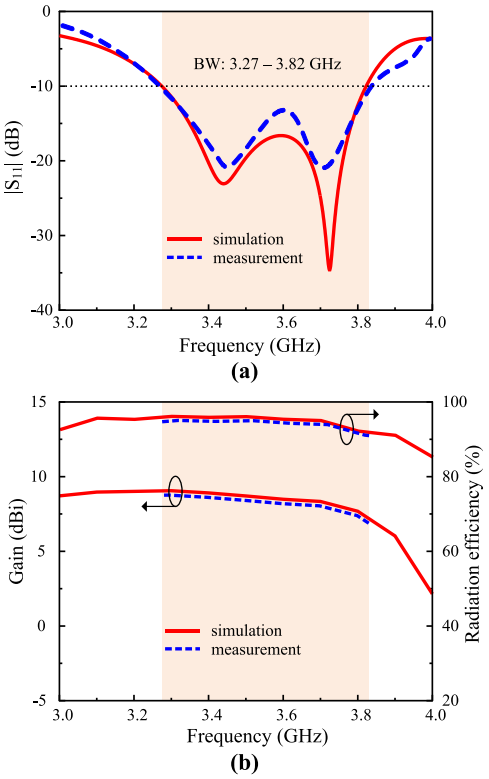

FIGURE 5. Results of the proposed single element antenna (a) $|S_{11}|$, (b) gain and radiation efficiency.

3) RADIATION PATTERNS

The simulated and measured radiation patterns of the single element antenna in xoz plane (H-plane) and yoz plane (E-plane) at different operating frequencies are shown in Fig. 6. The antenna offers stable and symmetrical radiation patterns having low side-lobe and back-lobe levels at all the investigated frequencies of 3.3, 3.5, and 3.7 GHz in the passband. The antenna shows a unidirectional radiation pattern with low back radiations.

III. MIMO ANTENNA DESIGN AND ISOLATION ENHANCEMENT

A. MIMO ANTENNA WITHOUT DECOUPLING STRUCTURE

The geometry and configuration of the MIMO antenna without decoupling structure is shown in Fig. 7, which consists of 4-single element antennas placed orthogonal to each other. The MIMO antenna is designed by translating the single-element, z-axis 90°, and other axes (x and y-axis) value of $(2 \times m) + g + i$ with repetition factor three. The optimized parameters for the antenna are as: $A = 146$ mm, $L = 19$ mm, $W = 14.5$ mm, $h_1 = h_2 = 1.524$ mm, $R = 5$ mm, $L_f = 11.6$ mm, $W_f = 3$ mm, $P = 17.6$ mm, $m = 16.4$ mm, $g = 1.2$ mm. This antenna offers low isolation and low gain, especially at higher frequency. The results are shown in later section. Therefore, a reduction of coupling between antennas is needed.

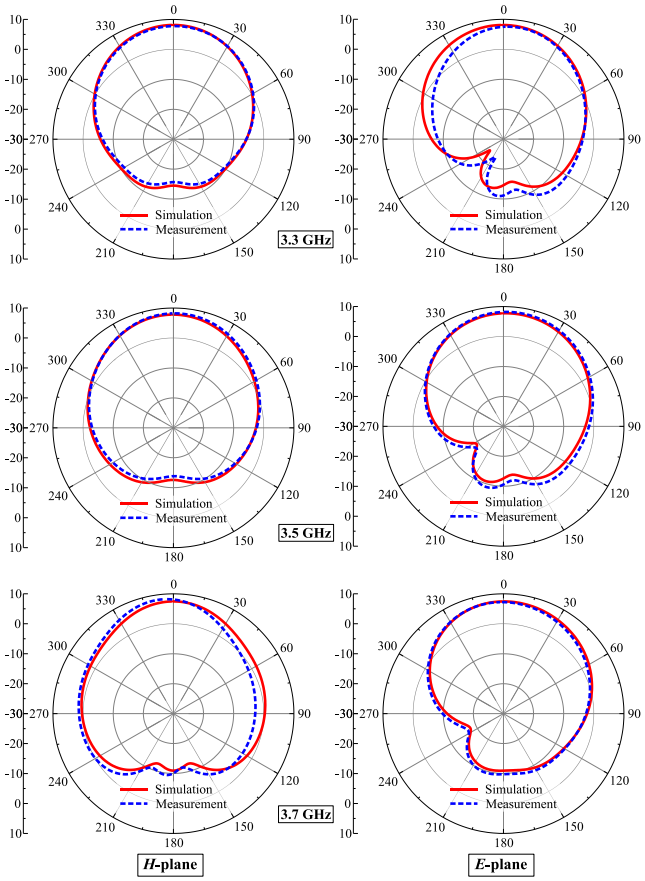

FIGURE 6. Radiation pattern of the proposed single element antenna with metasurface for different frequencies.

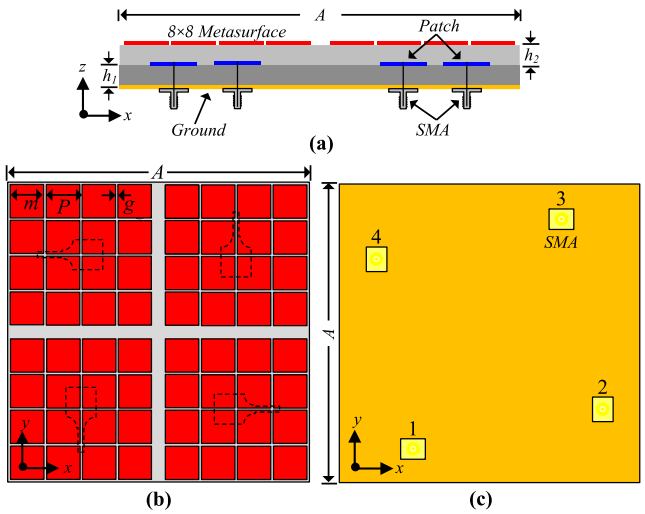

FIGURE 7. Geometry and configuration of the MIMO antenna without decoupling structure: (a) side view (b) top view of metasurface, and (c) ground plane.

B. THE PROPOSED MIMO ANTENNA WITH DECOUPLING STRUCTURE

The geometry and configuration of the proposed MIMO antenna with decoupling structure is shown in Fig. 8. To improve the isolation which is expressed by transmission-coefficient, a decoupling structure consisting of slots and shorting pins is designed. For designing the slot structure, the copper layer is etched from the ground plane by a width of 2.2 mm. The distance between two symmetric slots is 5.6 mm. By using this slot structure, isolation is improved. For further improvements, metallic strips of copper are designed with width and length of A and i, respectively, on the metasurface plane. Afterward, the metallic strips (located between MIMO elements) on the metasurface are connected to the ground plane via shorting pins through the substrates. The radius of the shorting pins is r. The electromagnetic field distribution is affected by these slots and shorting pins, and consequently, the mutual coupling is reduced. The optimized parameters for the proposed MIMO antenna are as: $A = 146$ mm, $L = 19$ mm, $W = 14.5$ mm, $h_1 = h_2 = 1.524$ mm, $R = 5$ mm, $L_f = 11.6$ mm, $W_f = 3$ mm, $s = 2$ mm, $E_s = 57.9$ mm, $P = 17.6$ mm, $m = 16.4$ mm, $g = 1.2$ mm, $i = 2.8$ mm, $j = 3$ mm, $k = 68$ mm, $d = 2.2$ mm, $D = 10$ mm and shorting pin radius $r = 0.75$ mm.

The isolation enhancement for different antenna structures is shown in Fig. 9. The transmission coefficient for adjacent antennas, $|S_{12}|$, $|S_{14}|$, $|S_{23}|$, and $|S_{34}|$ show identical curves. Moreover, the $|S_{13}|$ and $|S_{24}|$ curves are the same with lower values, since these antennas are located at the diagonal positions having longer distance among them compared to other adjacent antennas. The transmission coefficient for the adjacent antennas ($|S_{12}|$, $|S_{14}|$, $|S_{23}|$, and $|S_{34}|$) is shown in Fig. 9(a). It can be seen that without decoupling structure the average isolation is 18 dB and it suffers from strong mutual coupling at a higher frequency. By using the slot structure, the mutual coupling is reduced significantly in the upper-frequency region. MIMO antenna with the shorting pins shows similar results. While the proposed decoupling structure (combination of both slots and shorting pins) offers a significant isolation improvement at the entire operating frequency. For diagonal antennas ($|S_{13}|$ and $|S_{24}|$), the transmission coefficient is shown in Fig. 9(b). Without decoupling structure, the diagonal antennas show average low isolation of 23 dB. The slot structure offers improved isolation around 3.5 GHz. Similarly, the shorting pins reduce the mutual coupling between antenna elements and provide enhanced isolation at the entire operating frequency band. Finally, the proposed decoupling structure (combination of both slots and shorting pins), reduced the mutual coupling significantly and very high isolation between diagonal antennas is achieved at the entire frequency band. The highest isolation for MIMO antenna without decoupling structure is 26 dB for $|S_{12}|$, $|S_{14}|$, $|S_{23}|$, and $|S_{34}|$ parameters, while for the proposed MIMO antenna with decoupling structure, this value is reduced to 44 dB. The maximum isolation for antenna without decoupling structure for $|S_{13}|$ and $|S_{24}|$ is 30 dB, which is decreased to 72 dB for the proposed antenna.

By analyzing the surface current distribution, the effectiveness of the decoupling structure can be observed [29]. Fig. 10 shows the surface current distribution of the proposed

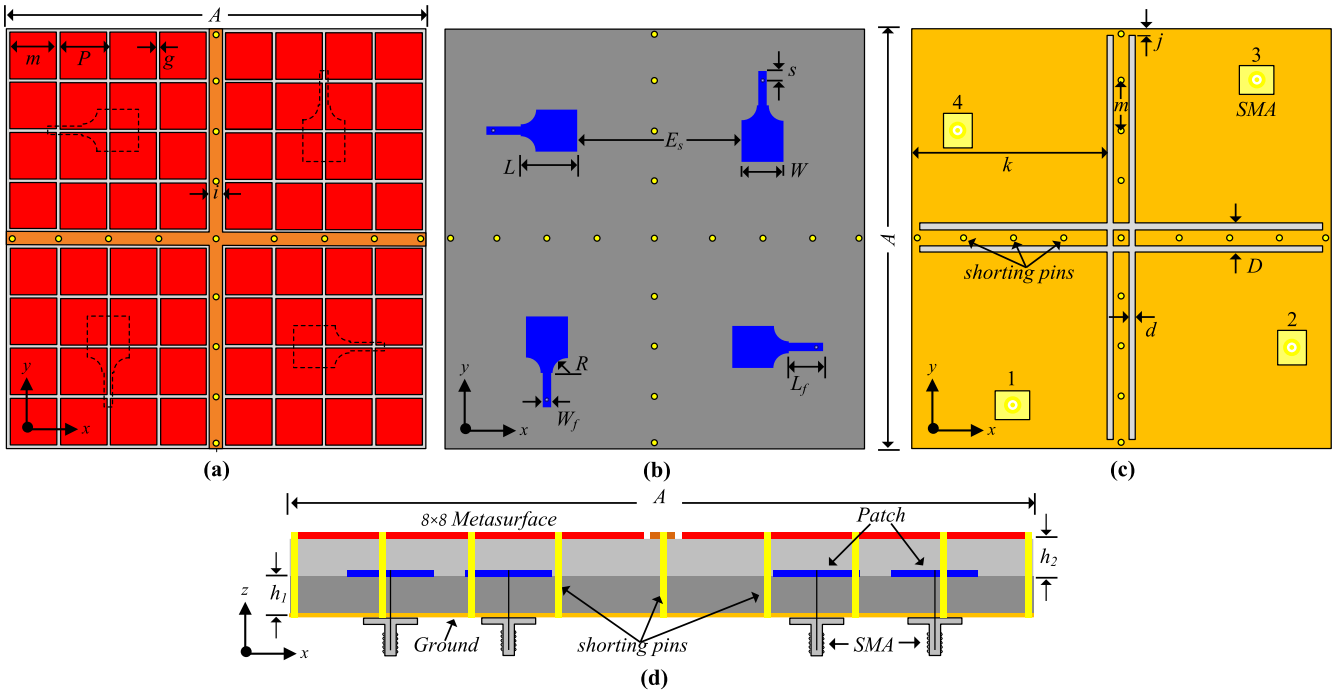

FIGURE 8. Geometry and configuration of the proposed MIMO antenna: (a) top view of metasurface (b) top view of the patch (c) ground plane, and (d) side view.

MIMO antenna at frequency 3.5 GHz for port-1 and port-3. From Fig. 10(a) when port-1 is excited, it can be visualized that without decoupling structure there is a strong current distribution that goes from the excited patch to the neighboring patches, thus the mutual coupling is very high. On the other hand, the strong current distribution to the adjacent patches is stopped by the decoupling structure, and hence, high isolation among MIMO antenna elements is achieved. To verify the same effect of decoupling structure, we have shown the surface current distribution for the excited port-3 in Fig. 10(b).

The gain of the proposed single element antenna and the proposed MIMO antenna (with and without decoupling structure) are shown in Fig. 11. The measured maximum gain of the proposed single element antenna is 8.1 dBi. However, due to mutual coupling between the MIMO elements, the MIMO without decoupling structure shows an unstable and low gain compared to the single element at high frequency band (3.5 – 4 GHz). The gain is decreased to 4 dBi due to high correlation. Using decoupling structure in the proposed MIMO antenna, mutual coupling is reduced between antenna elements and high isolation is achieved. Therefore, the proposed MIMO antenna shows a stable and high gain with a maximum value of 8.72 dBi. The gain of the proposed MIMO antenna is higher than the proposed single element antenna due to the increment of the radiating area in MIMO design. The gain curves of MIMO antenna configurations are only for port-1. All other ports of the proposed MIMO antenna show almost similar performance.

The detailed insight into the antenna design method and optimization process is summarized in the flowchart, shown in Fig. 12. The flowchart illustrates, how the antenna is constructed and what the significant design parameters play

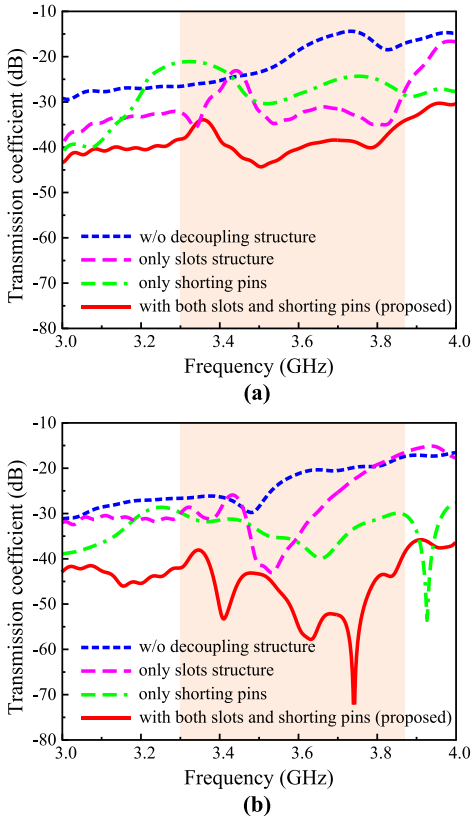

FIGURE 9. Transmission coefficient for different MIMO configuration (a) $|S_{12}|$, $|S_{14}|$, $|S_{23}|$, $|S_{34}|$, (b) $|S_{13}|$, and $|S_{24}|$.

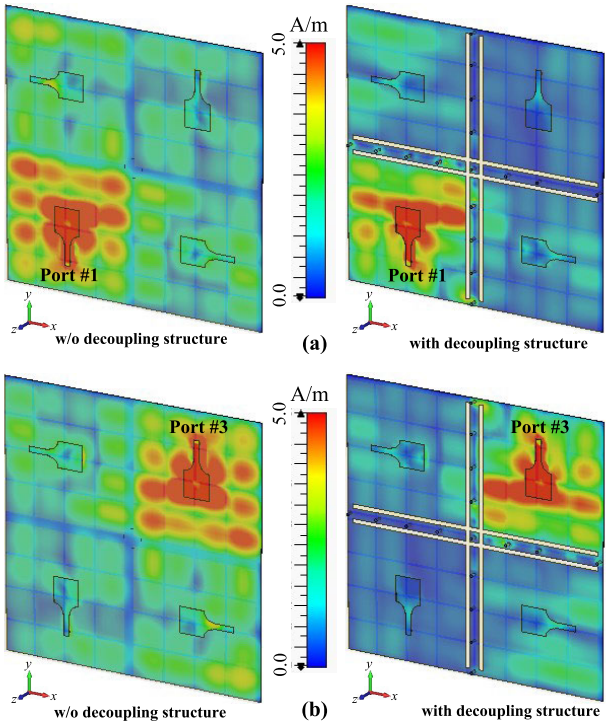

FIGURE 10. Surface current distribution with and without decoupling structure of different port excitation at 3.5 GHz (a) port-1 and (b) port-3.

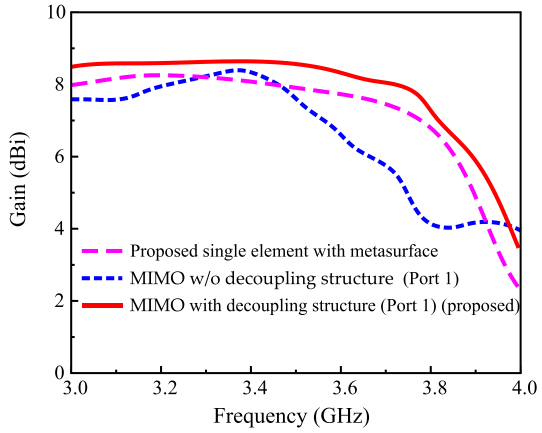

FIGURE 11. Gain of the proposed antennas for different configurations.

a role in the optimization of the antenna's gain and to achieve high isolation of the proposed MIMO antenna.

IV. PROPOSED MIMO ANTENNA RESULTS

To verify the design concept, a prototype of the proposed MIMO antenna is fabricated and measured. Its parts of assembly and the fabricated antenna is shown in Fig. 13(a) and the far-field measurement setup is shown in Fig. 13(b). With the help of an adhesive liquid the MTS layer is directly stacked on the MIMO patch radiators. PNA network analyzer (Agilent Technologies E8364B) was used to measure S-parameter in open air condition and the far-field radiation performance is measured and characterized by a commercial company [28]

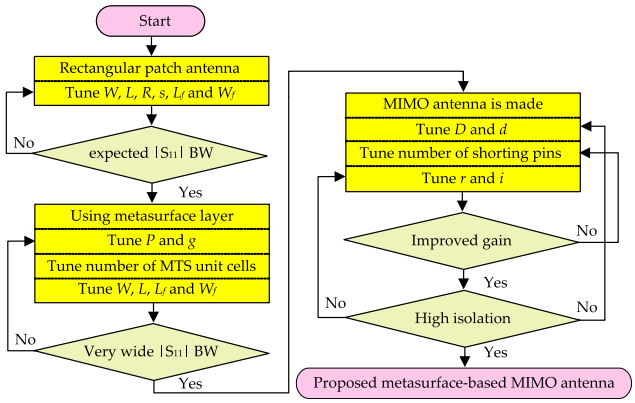

FIGURE 12. The design procedure and optimization of the proposed MIMO antenna.

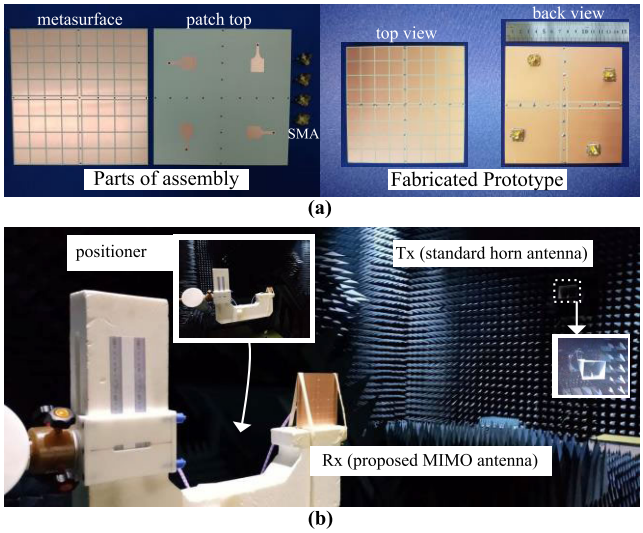

FIGURE 13. Photographs of the (a) fabricated MIMO antenna and its parts of the assembly, and (b) far-field measurements setup.

in an anechoic chamber. A well-calibrated standard gain horn antenna is used as a transmit (TX) antenna and the prototype is measured as a receiving (RX) antenna. Amplifiers are used to supply stable power reception. At the time of testing, the antenna is rotated to measure the radiation intensity at different orientations. To show the robustness of the MIMO antenna system, the MIMO diversity performance in terms of isolation, envelope correlation coefficient, and diversity gain are studied.

A. REFLECTION COEFFICIENT

The simulated and the measured reflection coefficient plots of the proposed Sub-6 GHz (n78 band) MIMO antenna is shown in Fig. 14. For isolation enhancement, some parameters are changed in MIMO antenna, thence the MIMO antennas have a little different 10 dB bandwidth than the proposed single-element antenna. It can be seen that the antenna has a good impedance matching in a wideband frequency range starting from 3.3 to 3.87 GHz, equivalent to a fractional

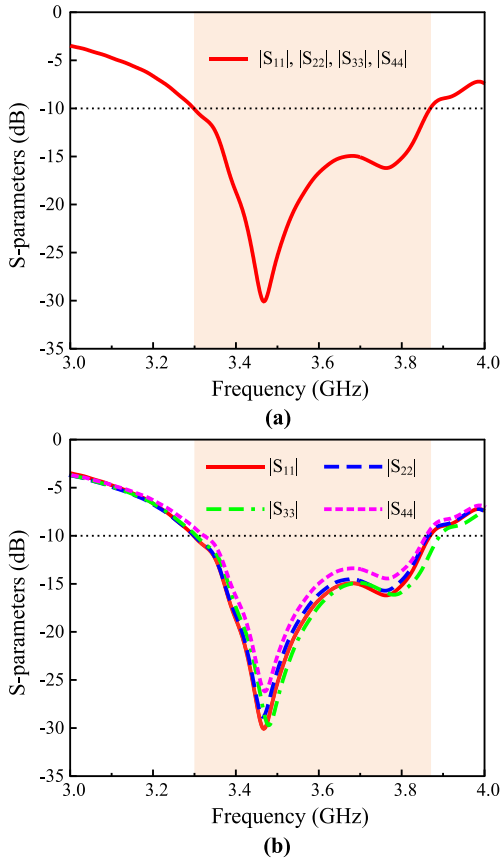

FIGURE 14. S-parameters of the proposed MIMO antenna (a) simulation and (b) measurement.

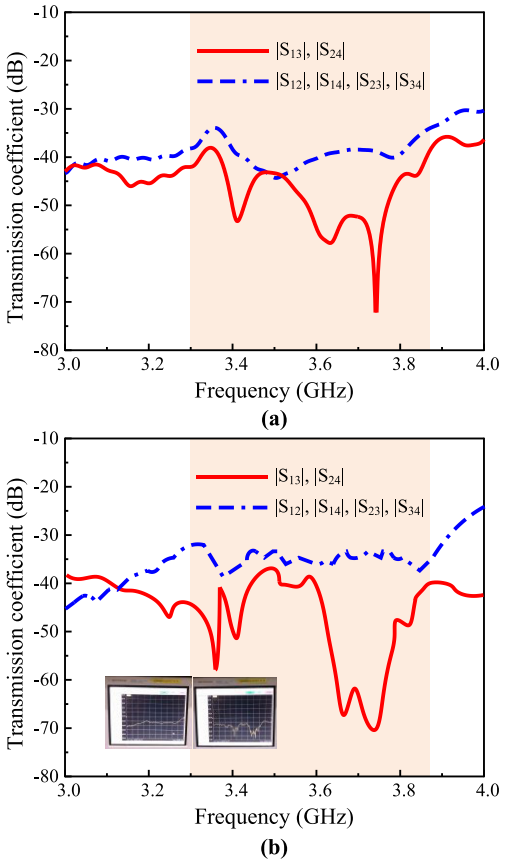

FIGURE 15. Transmission coefficient of the proposed MIMO antenna (a) simulation and (b) measurement.

bandwidth of 15.9% with respect to the central operating frequency. The antennas show almost the same reflection coefficient curves since all the antenna elements have symmetrical geometry and placement. A little difference in the measured reflection coefficients among the antenna elements is due to the measurement tolerances.

B. TRANSMISSION COEFFICIENT

The transmission coefficient is expressed as the mutual coupling between the MIMO elements. The simulated and measured transmission coefficients are plotted in Fig. 15. By using the proposed decoupling structure, the antennas show a high isolation characteristic. The minimum isolation of the antennas is >32 dB and maximum isolation is 72 dB in the entire operating bandwidth.

C. ENVELOPE CORRELATION COEFFICIENT (ECC)

The parameter that shows how much MIMO antennas are independent in their individual performance, for instance, radiation patterns and polarization is the envelope correlation coefficient (ECC) [30]. Equation (3) and (4) is used to compute the ECC (ρ_{eij}) for the MIMO antenna system both the S-parameters and far-field radiation respectively [20].

$$\rho_{eij} = \frac{|S_{ii}{*}S_{ij} + S_{ji} * S_{jj}|^2}{(1-|S_{ii}|^2 - S_{ij}^2)(1-\left|S_{ji}\right|^2 - S_{jj}^2)} \tag{3}$$

$$\rho_{eij} = \frac{|\int\int_0^{4\pi}\left[\vec{R}_i(\theta,\varphi) \times \vec{R}_j(\theta,\varphi)\right] d\Omega|^2}{\int\int_0^{4\pi}|\vec{R}_i(\theta,\varphi)|^2 d\Omega \int\int_0^{4\pi}|\vec{R}_j(\theta,\varphi)|^2 d\Omega} \tag{4}$$

Here, S_{ii} is the reflection coefficient and S_{ij} is the transmission coefficient. $\vec{R}_i(\theta,\varphi)$ and $\vec{R}_j(\theta,\varphi)$ are the three-dimensional radiation patterns of i^{th} and j^{th} antenna and Ω is the solid angle. For the proposed MIMO antenna, the ECC values obtained from (3) and (4) are very low (less than0.001) within the operating frequency. This excellent diversity performance of the proposed MIMO antenna is shown in Fig. 16.

D. DIVERSITY GAIN (DG)

Another fundamental parameter that describes the effect of the diversity scheme on the radiated power is the diversity gain (DG). In Fig. 17, the diversity gain (DG) of the proposed MIMO antenna is shown and computed as a function of frequency using the relation in equation 5 [20].

$$Diversity\ Gain = 10\sqrt{1-|\rho_{eij}|^2} \tag{5}$$

TABLE 1. Comparison of the proposed MIMO antenna with state-of-the-art works.

Ref.	Isolation Enhancement Techniques	BW (%)	Peak Gain (dBi)	Radiation Efficiency	Min. isolation (dB)	Max. isolation (dB)
[12]	Parasitic PCI (polarization-conversion isolator)	3.6	Not given	63%	≥ 25	33
[13]	Parasitic structures with square-ring slot radiator	11.1	6.5	62 – 78%	≥ 15	29
[14]	Uni-conductor electromagnetic bandgap (UC-EBG)	10.3	4.3	63%	≥ 32	71
[15]	Fractal-shape EBG	5.0	5	Not given	≥ 30	50
[16]	Multi-layered EBG	5	Not given	Not given	≥ 25	50
[17]	MSS loading and mutual decoupling structure	9.3	8.3	68%	≥ 15	33
[18]	3-D meta-material structures	4.1	5	Not given	≥ 18	33
[19]	Near-field resonators (NFR)	6.1	5.11	80%	≥ 20	25
Prop.	**Slots & shorting pins**	**15.9**	**8.72**	**92 – 96%**	**≥ 32**	**72**

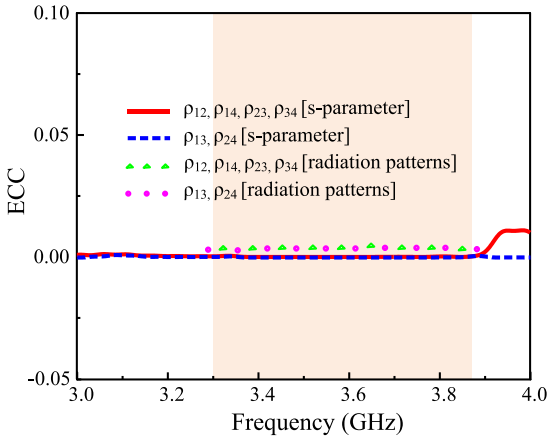

FIGURE 16. Envelope correlation coefficient (ECC) of the proposed MIMO antenna.

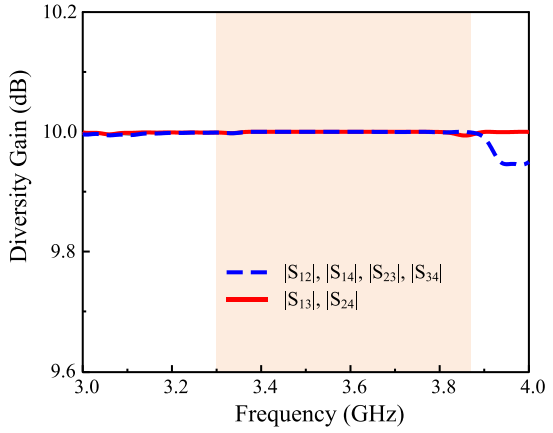

FIGURE 17. Diversity gain of the proposed MIMO antenna.

For all the antenna elements, the diversity gain of the proposed MIMO antenna is more than 9.98 dB which is very close to the ideal value of 10 dB.

E. COMPARISON WITH STATE-OF-THE-ART WORKS

Table 1 shows the performance comparison of the proposed MIMO antenna with the existing similar MIMO microstrip patch structures with high isolation. The comparison is made with respect to different performance metrics including isolation enhancement techniques, bandwidth, peak gain, radiation efficiency, minimum isolation, and maximum isolation. Many appealing designs of MIMO antenna with isolation improvement techniques were reported in [12-19].

It can be seen that decoupling structure can lead to a better maximum value of isolation, particularly [12], [14], [15], [19]. However, these designs suffer from narrow bandwidth. In comparison, by operating bandwidth with a competitive isolation feature, our architecture is dominant. In addition, the proposed MIMO antenna offers a very high radiation efficiency with a high gain, while maintaining high isolation between antenna elements.

V. CONCLUSION

A metasurface-based multiple-input multiple-output antenna (MIMO antenna) with wideband operation is presented for 5G Sub-6 GHz (n78 band) applications. The antenna is sandwiched between an 8×8 metallic square cell metasurface and a finite ground plane. Rectangular patch fed by a microstrip line is the main radiating element, whose lower ends are truncated with a semicircle. The distinguishing feature of this design is high isolation between MIMO antenna elements while maintaining high gain and wideband characteristics. The proposed single element antenna geometry has an overall compact size of $0.85\lambda_0 \times 0.85\lambda_0 \times 0.038\lambda_0$. Simulated and measured results show that the proposed single element antenna has a wide 10 dB impedance bandwidth of 15.5% (3.27 – 3.82 GHz). The antenna also offers stable and symmetrical radiation patterns with a high radiation efficiency (>92%) and a peak gain of 8.1 dBi. The proposed

4-port (2 × 2) MIMO antenna is designed using the proposed single element by placing each element orthogonally to each other. A decoupling structure consisting of slots and metallic strip with shorting pins is implemented to improve the isolation between the MIMO elements. The proposed decoupling structure stopped the strong current distribution to the adjacent patches that reduce the mutual coupling and hence, high isolation between MIMO antenna elements is achieved. For experimental validation, a prototype of the proposed 4 port (2×2) MIMO antenna with an overall volume of $1.75\lambda_0 \times 1.75\lambda_0 \times 0.038\lambda_0$ is fabricated and measured. The simulated and measured result indicates that the proposed MIMO antenna has a wide 10 dB impedance bandwidth of 15.9% (3.3 – 3.87 GHz) with a peak gain of 8.72 dBi. The proposed MIMO antenna offers excellent diversity performance in terms of isolation between antenna elements (>32dB), envelope correlation coefficient (less than 0.001), and diversity gain (9.99 dB). These features of the proposed antenna system make it a suitable candidate for 5G Sub-6 GHz (n78 band) MIMO systems.

REFERENCES

[1] L. Gavrilovska, V. Rakovic, and V. Atanasovski, "Visions towards 5G: Technical requirements and potential enablers," *Wireless Pers. Commun.*, vol. 87, no. 3, pp. 731–757, Apr. 2016.

[2] T. S. Rappaport, S. Sun, R. Mayzus, H. Zhao, Y. Azar, K. Wang, G. N. Wong, J. K. Schulz, M. Samimi, and F. Gutierrez, "Millimeter wave mobile communications for 5G cellular: It will work," *IEEE Access*, vol. 1, pp. 335–349, 2013.

[3] *Federal Communications Commission. America's 5G Future*. Accessed: Mar. 16, 2021. [Online]. Available: https://www.fcc.gov/5G

[4] Qualcomm Technologies Inc. (Dec. 2020). *Spectrum for 4G and 5G*. Accessed: Mar. 16, 2021. [Online]. Available: https://www.qualcomm.com/media/documents/files/spectrum-for-4g-and-5g.pdf

[5] N. O. Parchin, H. J. Basherlou, Y. I. A. Al-Yasir, A. Ullah, R. A. Abd-Alhameed, and J. M. Noras, "Multi-band MIMO antenna design with user-impact investigation for 4G and 5G mobile terminals," *Sensors*, vol. 19, no. 3, p. 456, Jan. 2019.

[6] Y. Zhang, J.-Y. Deng, M.-J. Li, D. Sun, and L.-X. Guo, "A MIMO dielectric resonator antenna with improved isolation for 5G mm-wave applications," *IEEE Antennas Wireless Propag. Lett.*, vol. 18, no. 4, pp. 747–751, Apr. 2019.

[7] N. O. Parchin, H. J. Basherlou, Y. I. A. Al-Yasir, A. M. Abdulkhaleq, and R. A. Abd-Alhameed, "Ultra-wideband diversity MIMO antenna system for future mobile handsets," *Sensors*, vol. 20, no. 8, p. 2371, Apr. 2020.

[8] Z. Li, Z. Du, M. Takahashi, K. Saito, and K. Ito, "Reducing mutual coupling of MIMO antennas with parasitic elements for mobile terminals," *IEEE Trans. Antennas Propag.*, vol. 60, no. 2, pp. 473–481, Feb. 2012.

[9] M. S. Khan, A. Capobianco, A. I. Najam, I. Shoaib, E. Autizi, and M. F. Shafique, "Compact ultra-wideband diversity antenna with a floating parasitic digitated decoupling structure," *IET Microw., Antennas Propag.*, vol. 8, no. 10, pp. 747–753, Jul. 2014.

[10] S. Zhang, Z. Ying, J. Xiong, and S. He, "Ultrawideband MIMO/diversity antennas with a tree-like structure to enhance wideband isolation," *IEEE Antennas Wireless Propag. Lett.*, vol. 8, pp. 1279–1282, Nov. 2009.

[11] L. Kang, H. Li, X. Wang, and X. Shi, "Compact offset microstrip-fed MIMO antenna for band-notched UWB applications," *IEEE Antennas Wireless Propag. Lett.*, vol. 14, pp. 1754–1757, Apr. 2015.

[12] Y.-F. Cheng, X. Ding, W. Shao, and B.-Z. Wang, "Reduction of mutual coupling between patch antennas using a polarization-conversion isolator," *IEEE Antennas Wireless Propag. Lett.*, vol. 16, pp. 1257–1260, Nov. 2017.

[13] N. O. Parchin, Y. I. A. Al-Yasir, A. H. Ali, I. Elfergani, J. M. Noras, J. Rodriguez, and R. A. Abd-Alhameed, "Eight-element dual-polarized MIMO slot antenna system for 5G smartphone applications," *IEEE Access*, vol. 7, pp. 15612–15622, 2019.

[14] I. Mohamed, M. Abdalla, and A. E.-A. Mitkees, "Perfect isolation performance among two-element MIMO antennas," *AEU Int. J. Electron. Commun.*, vol. 107, pp. 21–31, Jul. 2019.

[15] M. Naderi, F. B. Zarrabi, F. S. Jafari, and S. Ebrahimi, "Fractal EBG structure for shielding and reducing the mutual coupling in microstrip patch antenna array," *AEU Int. J. Electron. Commun.*, vol. 93, pp. 261–267, Sep. 2018.

[16] T. Jiang, T. Jiao, and Y. Li, "A low mutual coupling MIMO antenna using periodic multi-layered electromagnetic band gap structures," *Appl. Comput. Electromagn. J.*, vol. 33, no. 1, pp. 305–311, Mar. 2018.

[17] S. Luo, Y. Li, Y. Xia, and L. Zhang, "A low mutual coupling antenna array with gain enhancement using metamaterial loading and neutralization line structure," *Appl. Comput. Electromagn. J.*, vol. 34, no. 3, pp. 411–418, Mar. 2019.

[18] K. Yu, Y. Li, and X. Liu, "Mutual coupling reduction of a MIMO antenna array using 3-D novel meta-material structures," *Appl. Comput. Electromagn. J.*, vol. 33, no. 7, pp. 758–763, Jul. 2018.

[19] M. Li, B. G. Zhong, and S. W. Cheung, "Isolation enhancement for MIMO patch antennas using near-field resonators as coupling-mode transducers," *IEEE Trans. Antennas Propag.*, vol. 67, no. 2, pp. 755–764, Feb. 2019.

[20] N. Hussain, M.-J. Jeong, A. Abbas, and N. Kim, "Metasurface-based single-layer wideband circularly polarized MIMO antenna for 5G millimeter-wave systems," *IEEE Access*, vol. 8, pp. 130293–130304, 2020.

[21] J. G. Lee, C. H. Lee, and J. H. Lee, "One-dimensionally polarization-independent retrodirective metasurface," *J. Electromagn. Eng. Sci.*, vol. 20, no. 1, p. 80, Jan. 2020.

[22] N. Hussain, U. Azimov, J.-W. Park, S.-Y. Rhee, and N. Kim, "A microstrip patch antenna sandwiched between a ground plane and a metasurface for WiMAX applications," in *Proc. Asia–Pacific Microw. Conf. (APMC)*, Nov. 2018, pp. 1016–1018.

[23] S. X. Ta and I. Park, "Low-profile broadband circularly polarized patch antenna using metasurface," *IEEE Trans. Antennas Propag.*, vol. 63, no. 12, pp. 5929–5934, Dec. 2015.

[24] N. Hussain, M.-J. Jeong, A. Abbas, T.-J. Kim, and N. Kim, "A metasurface-based low-profile wideband circularly polarized patch antenna for 5G millimeter-wave systems," *IEEE Access*, vol. 8, pp. 22127–22135, 2020.

[25] *Antenna Theory: Analysis and Design*, 3rd ed. Hoboken, NJ, USA: Wiley, 2005, pp. 811–820.

[26] F. Costa, O. Luukkonen, C. R. Simovski, A. Monorchio, S. A. Tretyakov, and P. M. de Maagt, "TE surface wave resonances on high-impedance surface based antennas: Analysis and modeling," *IEEE Trans. Antennas Propag.*, vol. 59, no. 10, pp. 3588–3596, Oct. 2011.

[27] X. Li, J. Yang, Y. Feng, M. Yang, and M. Huang, "Compact and broadband antenna based on a step-shaped metasurface," *Opt. Exp.*, vol. 25, no. 16, pp. 19023–19033, Aug. 2017.

[28] *EMTI Homepage*. Accessed: Dec. 10, 2020. [Online]. Available: http://emti.or.kr/

[29] H. H. Tran and N. Nguyen-Trong, "Performance enhancement of MIMO patch antenna using parasitic elements," *IEEE Access*, vol. 9, pp. 30011–30016, 2021.

[30] S.-H. Kim and J.-Y. Chung, "Analysis of the envelope correlation coefficient of MIMO antennas connected with suspended lines," *J. Electromagn. Eng. Sci.*, vol. 20, no. 2, pp. 83–90, Apr. 2020.

MD. ABU SUFIAN (Graduate Student Member, IEEE) received the B.S. degree in electrical and electronic engineering from American International University-Bangladesh (AIUB), Dhaka, Bangladesh, in 2020. He is currently pursuing an Integrated Ph.D. degree in information and communication engineering from Chungbuk National University, Cheongju, South Korea. He is a member of IEEE Antennas & Propagation Society (IEEE APS). His research interests include antenna design for 5G mobile communication, MIMO systems, metasurface antennas, satellite communication, and BioEM effects of antennas.

NIAMAT HUSSAIN received the B.S. degree in electronics engineering from the Dawood University of Engineering and Technology, Karachi, Pakistan, in 2014, the M.S. degree in electrical and computer engineering from Ajou University, Suwon, South Korea, and the Ph.D. degree in information and communication engineering from Chungbuk National University, Cheongju, South Korea. He is currently a Postdoctoral Researcher with Chungbuk National University. His research interests include lens-coupled antennas, metasurface antennas, metamaterial antennas, UWB antennas, mmWave antennas, and terahertz antennas. He was bestowed with the Best Paper Award, in 2017, for his presented paper at Korea Winter Conference.

HUSSAIN ASKARI received the B.S. degree in telecommunication engineering from The Islamia University of Bahawalpur, Pakistan, in 2017. He is currently pursuing the master's degree in information and communication engineering with Chungbuk National University, Cheongju, South Korea. His research interests include circularly polarized antennas, metamaterial antennas, UWB antennas, mmWave antennas, BioEM effects of antennas, and terahertz antennas.

SEONG GYOON PARK is currently serving as a Professor with the Department of Information and Communication Engineering, Kongju National University. His research interests include EMC, antenna design for WIFI, and mobile communications.

KOOK SUN SHIN received the B.S. degree in electronic and communication engineering from the Korea National University of Transportation, South Korea, in 2001, and the M.S. degree in information and communication engineering from Chungbuk National University, Cheongju, South Korea, in 2003, where he is currently pursuing the Ph.D. degree with the Department of Information and Communication Engineering. He is currently working at FITI Testing & Research Institute, Cheongju. His research interests include antenna design, EMC measurements, and EMF.

NAM KIM received the B.S., M.S., and Ph.D. degrees in electronics engineering from Yonsei University, Seoul, South Korea, in 1981, 1983, and 1988, respectively. He has been a Professor with the School of Information and Communication Engineering, Chungbuk National University, Cheongju, South Korea, since 1989. His research interests include optical information processing, the health effect of the EMF, wireless power transfer, and antennas for mobile communications. He is a member of the International Advisory Committee for the World Health Organization Project on EMF, the IEEE International Committee on Electromagnetic Safety, and the International Electro Technical Commission TC 106. He was the President of the Bioelectromagnetics Society.